July 24, 2023

Synthesis, X-ray Structures, and Optical and Magnetic Properties of Cu(II) Octafluoro-octakisperfluoro(isopropyl)phthalocyanine: The Effects of Electron Addition and Fluorine Accretion

Maxim A. Faraonov, *Russian Academy of Sciences*
Ilya A. Yakushev, *Russian Academy of Sciences*
Evgeniya I. Yudanova, *Russian Academy of Sciences*
Marius Pelmus, *Seton Hall University*
Sergiu M. Gorun, *Seton Hall University*, et al.

Inorganic Chemistry

pubs.acs.org/IC

Article

Synthesis, X-ray Structures, and Optical and Magnetic Properties of Cu(II) Octafluoro-octakisperfluoro(isopropyl)phthalocyanine: The Effects of Electron Addition and Fluorine Accretion

Maxim A. Faraonov,* Ilya A. Yakushev, Evgeniya I. Yudanova, Marius Pelmus, Sergiu M. Gorun,* Akihiro Otsuka, Hideki Yamochi, Hiroshi Kitagawa, and Dmitri V. Konarev*

Cite This: *Inorg. Chem.* 2023, 62, 11390−11401

Read Online

ACCESS | Metrics & More | Article Recommendations | Supporting Information

ABSTRACT: The stepwise reduction of copper(II) 1,4,8,11,15,18,22,25-octafluoro-2,3,9,10,16,17,23,24-octakisperfluoro(isopropyl) phthalocyanine ($Cu^{II}F_{64}Pc$) in *o*-dichlorobenzene ($C_6H_4Cl_2$) by potassium graphite in the presence of cryptand(K^+), abbreviated L^+, results in the formation of $(L^+)[Cu^{II}(F_{64}Pc^{\bullet 3-})]^-\cdot 2C_6H_4Cl_2$ (**1**), $(L^+)_2[Cu^{II}(F_{64}Pc^{4-})]^{2-}\cdot C_6H_4Cl_2$ (**2**), and $(L^+)_2[Cu^{II}(F_{64}Pc^{4-})]^{2-}$ (**3**) complexes. Single-crystal X-ray structures revealed their composition and a monotonic increase with increased phthalocyanine (Pc) negative charges of the magnitude of alternative shortening and elongation of the prior equivalent $N_{meso}-C$ bonds. The complexes are separated by bulky *i*-C_3F_7 substituents, large cryptand counterions, and solvent molecules. Weak, new bands are generated in the visible and near-infrared (NIR) domains upon reductions. The one-electron reduced complex, $[Cu^{II}(F_{64}Pc^{\bullet 3-})]^-$, is a diradical, exhibiting broad electron paramagnetic resonance (EPR) signals, with intermediate parameters between those typical to Cu^{II} and $F_{64}Pc^{\bullet 3-}$. The two-electron reduced complexes, $[Cu^{II}(F_{64}Pc^{4-})]^{2-}$, contain a diamagnetic $F_{64}Pc^{4-}$ macrocycle and a single spin, $S = 1/2$, on Cu^{II}. The bulky perfluoroisopropyl groups are suppressing intermolecular $\pi-\pi$ interactions between Pcs in the $[Cu^{II}(F_{64}Pc^{n-})]^{(n-2)-}$ (n = 3, 4) anions, **1**−**3**, similar to the case of the nonreduced complex. However, $\pi-\pi$ interactions between **1** and *o*-dichlorobenzene are observed. The d^9 and Pc electrons in **1** are antiferromagnetically coupled, $J = -0.56$ cm^{-1}, as revealed by superconducting quantum interference device (SQUID) magnetometry, but the coupling is at least 1 order of magnitude smaller compared with the coupling observed for $Cu^{II}(F_8Pc^{\bullet 3-})$ and $Cu^{II}(F_{16}Pc^{\bullet 3-})$, a testimony to the F accretion effect of rendering the Pc macrocycle progressively more electron-deficient. The data for $Cu^{II}(F_{64}Pc)$ provide structural, spectroscopic, and magnetochemical insights, which establish a trend of the effects of fluorine and charge variations of fluorinated Pcs within the macrocycle series $Cu^{II}(F_xPc)$, x = 8, 16, 64. Diamagnetic Pcs might be useful for photodynamic therapy (PDT) and related biomedical applications, while the solvent-processable biradicalic nature of the monoanion salts may constitute the basis for designing robust, air-stable electronic, and magnetically condensed materials.

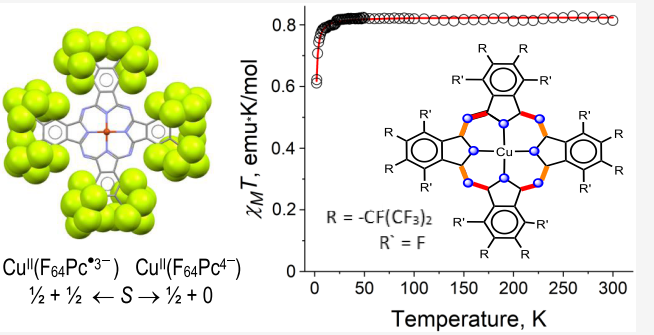

INTRODUCTION

The phthalocyanines (Pcs) are a large family of macrocycle compounds used as industrial dyes, currently investigated as materials for optical, electronic, and photoelectronic devices, catalysts, phototherapeutic drugs, and other biomedical applications.[1−10] Their properties can be effectively and rationally tuned by variations of the central atoms, axial ligands, and macrocycle substituents to yield both electron-rich and electron-poor macrocycles with potential wide and diverse applications. The introduction of strong electron-withdrawing substituents leads to a positive shift of the Pcs reduction potentials stabilizing their anionic species, including in air.[11] The largest redox shift has been achieved to date by the introduction of eight, bulky perfluoro(isopropyl) (*i*-C_3F_7) groups at the peripheral positions of perfluoro Pcs, forming 1,4,8,11,15,18,22,25-octafluoro-2,3,9,10,16,17,23,24-octakisperfluoro(isopropyl)phthalocyanine, present in $MF_{64}Pc$, M = Cu^{II}, Co^{II}, Zn^{II}, $V^{IV}O$, etc. The complexes enhanced solubility in organic solvents, and chemical stability rendered them suitable for applications in photodynamic therapy,[12,13] catalysis,[14−18] and materials for electrochromic displays.[19−22] Their strong electron acceptor ability allows the reversible addition of 1 or 2 electrons to form $[M(F_{64}Pc^{\bullet 3-})]^-$ or $[M(F_{64}Pc^{4-})]^{2-}$, while electron loss is suppressed.[13,19,20,23]

Received: March 17, 2023
Published: July 12, 2023

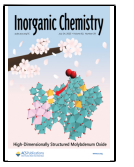

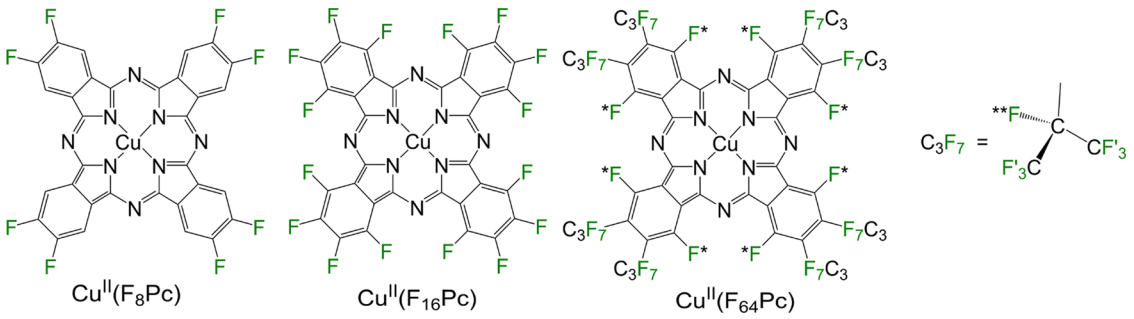

Figure 1. Structures of F_xPc^{n-} copper complexes. The degree and type of fluorination range from half-aromatic F, $x = 8$, to full aromatic F, $x = 16$, to half-perfluoroalkyl and half-aromatic F, $x = 64$.

Reduction or oxidation of Pcs yield species with an unpaired electron delocalized over the macrocycles. This electron can participate in the magnetic coupling of spins or high conductivity.[24,25] Moreover, in the case of paramagnetic central metal atoms, an unpaired electron localized on metal can interact with the conducting electron delocalized over the macrocycles leading to giant magnetoresistance.[26,27] Generally, metal phthalocyanine anions are very air-sensitive due to strongly negative reduction potentials[11] but that is not true for the air-stable radical trianions $F_{64}Pc^{\bullet 3-}$. Therefore, the $[M(F_{64}Pc^{\bullet 3-})]^-$ species can serve as components in magnetic, conducting, magneto-, and electro-optical devices working in air. Paramagnetic ions, such as Cu(II), are of special interest for electrochemically coupled magnetic interactions since copper(II) complexes have two magnetic centers in monoanionic species, viz. $[Cu^{II}(\text{macrocycle})^{\bullet 3-}]^-$.[28−31]

The effect of fluorination as a tool for the rational design of new materials with predictable structural, spectroscopic, magnetic properties, and reactivity is of interest.

We report here the stepwise 1- and 2-electron reductions of $Cu^{II}(F_{64}Pc)$ to form anions, crystal growth, and structural characterization of the anions complexed with potassium cryptand counterions, the optical and magnetic properties of the new materials, and resulting trends imparted by electron addition and fluorine accretion.

RESULTS AND DISCUSSION

The structures of F_xPc^{n-} copper complexes are shown in Figure 1, $x = 8$, 16, and 64 and $n = 2$, 3, and 4.

The fluorine atoms are labeled separately based on their positions in the molecule. As shown in Figure 1, for $x = 8$, only the peripheral type F is present; 2 types are present for $x = 16$: peripheral and nonperipheral; and 3 types of F are present for $x = 64$: primary (labeled with ′), tertiary F (labeled with **), and aromatic, nonperipheral (labeled with *).

The chemical composition of the complexes with $x = 64$ is shown in Table 1. For complexes **1**−**3**, reported here, the counterions and solvated molecules are also shown, as revealed by their single-crystal X-ray structures (see below). The reduction degree of the ligand, relative to $F_{64}Pc^{2-}$, is also shown.

Table 1. Chemical Composition of Cu(II) Complexes of the $F_{64}Pc$ Ligand[a]

Label	Formula, X-ray crystals	$F_{64}Pc^{2-}$ extra charge
0	$[Cu^{II}(F_{64}Pc^{2-})(C_4H_8O_2)_2]$	0
1	$\{\text{cryptand}(K^+)\}[Cu^{II}(F_{64}Pc^{\bullet 3-})]^-\cdot 2C_6H_4Cl_2$	−1
2	$\{\text{cryptand}(K^+)\}_2[Cu^{II}(F_{64}Pc^{4-})]^{2-}\cdot C_6H_4Cl_2$	−2
3	$\{\text{cryptand}(K^+)\}_2[Cu^{II}(F_{64}Pc^{4-})]^{2-}$	−2

[a]Cryptand: 4,7,13,16,21,24-hexaoxa-1,10-diazabicyclo[8.8.8]-hexacosane; $C_4H_8O_2$: ethyl acetate; $C_6H_4Cl_2$: *o*-dichlorobenzene.

Anionic salts **1**−**3** were prepared by reducing the parent complex, $[Cu^{II}(F_{64}Pc^{2-})]$, **0**, with potassium graphite (KC_8) in *o*-dichlorobenzene in the presence of 1 or 2 equiv of 4,7,13,16,21,24-hexaoxa-1,10-diazabicyclo[8.8.8]hexacosane cryptand. The previously reported reductions of $Cu^{II}(F_xPc)$ to $[Cu^{II}(F_xPc)^{\bullet 3-}]^-$ and $[Cu^{II}(F_xPc)^{4-}]^{2-}$ ($x = 8$, 16)[28,29] were performed with sodium fluorenone ketyl, $E_{redox} = -1.30$ V vs saturated calomel electrode (SCE),[32] or with sodium cyclopentadienyl cobalt dicarbonyl $(Na^+)[CpCo(CO)_2]^-$, $E_{redox} = -1.85$ V vs SCE, also in the presence of the cryptand.[29] For $x = 64$, KC_8 afforded the selective reduction of $[Cu^{II}(F_{64}Pc^{2-})]$ by 1 or 2 electrons. The anions are paired with cryptand(K^+) cations. The monoreduced complex **1** is deep-blue in *o*-dichlorobenzene, yielding large, black X-ray quality prismatic crystals with a characteristic copper luster by the slow diffusion of *n*-hexane over a period of 1−2 months. The composition of **1** was determined by X-ray diffraction and was supported by elemental analysis (see the Experimental Section). The reduction of **0** by two equivalents of cryptand affords the isolation of **3** as small, black, elongated plates, but only in extremely low yield. These crystals belong only to a single crystal phase, and here we present only the crystal structure of **3**. A different strategy was used to obtain complex **2**. Thus, one equivalent of cryptand and KC_8 was added to the solution that generated **1**, and the stirring continued for 24 h giving a red-violet solution, from which **2** could be isolated as a crystalline material in a small yield after 1 month of diffusion of *n*-hexane. We determined the crystal structure of **2** and studied its electron paramagnetic resonance (EPR) and optical properties using several single crystals, which were tested by X-ray diffraction and were shown to have the same unit cell parameters as **2**. Compositions of **2** and **3** were determined by X-ray diffraction. The continuation of the titration with a third equivalent of cryptand and KC_8 yielded a blue-pink solution, but no crystalline products could be isolated in this case.

These results are consistent with the following rationalization. Metal phthalocyanines are relatively weak electron acceptors, but their ability to accept electrons can be increased by the introduction of electron-withdrawing substituents. The substitution of aromatic hydrogen in $H_{16}Pc$ with fluorine indeed enhances the electronic-accepting capability of the Pc, as well as its thermal and chemical robustness, beneficial properties for catalytic applications. The formal replacement of the eight peripheral F atoms of $F_{16}PcCu$ with *iso*-C_3F_7-groups, to give $F_{64}PcCu$, shifts the redox potentials of $Cu^{II}F_xPc$ toward

https://doi.org/10.1021/acs.inorgchem.3c00887
Inorg. Chem. 2023, 62, 11390−11401

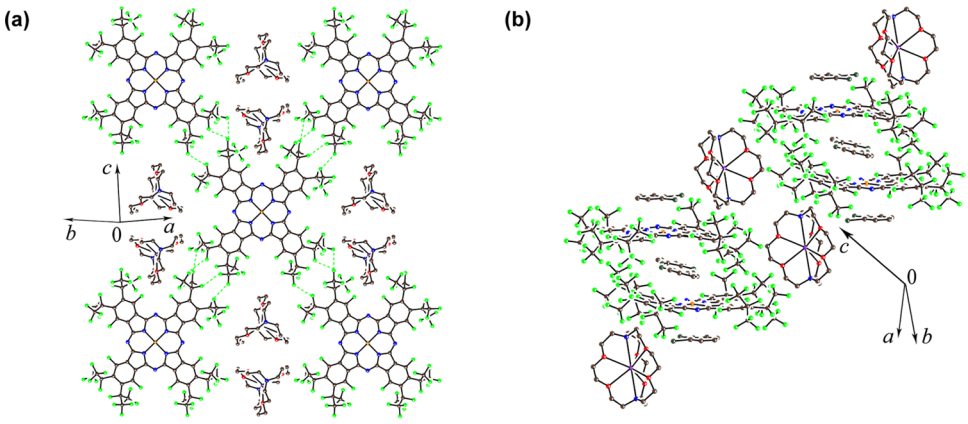

Figure 2. X-ray structure of **1**. Short van der Waals contacts are shown by green, dashed lines. (a) View, in projection, perpendicular to the Pc layers, showing the cations, but omitting the solvents for the sake of clarity. (b) View, approximately parallel to the Pc layers, showing both the cations and the intercalated *o*-dichlorobenzene solvent. Additional views are presented in Figure S1a–c, Supporting Information.

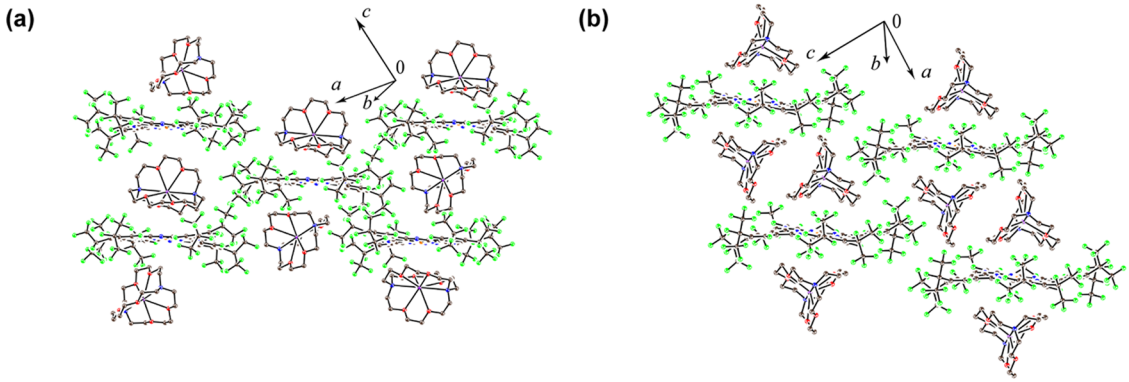

Figure 3. Crystal structures of complexes containing $\{cryptand(K^+)\}_2[Cu^{II}(F_{64}Pc^{4-})]^{2-}$. The viewing direction is approximately parallel to the Pc layers. The *o*-dichlorobenzene solvent in **2** has been omitted. Additional views are presented in Figure S1d–f for **2** and Figure S1g–i for **3**. (a) $\{cryptand(K^+)\}_2[Cu^{II}(F_{64}Pc^{4-})]^{2-}\cdot C_6H_4Cl_2$, **2**. (b) $\{cryptand(K^+)\}_2[Cu^{II}(F_{64}Pc^{4-})]^{2-}$, **3**.

even more positive values.[13,19,20,23] A positive shift of about 0.4 V is observed for the $F_{64}Pc$ scaffold vs $F_{16}Pc$. Notably, the positive shift is metal-independent[34] since the frontier orbitals consist of an atomic orbital of the ligand.

Naturally, the ligand-based frontier orbitals are susceptible to variations in ligand substituents. The perfluoroalkyl substituents exert a higher inductive effect compared with the aromatic F atoms, as the positive dipole of CF_3 groups creates positive potential on adjacent atoms.[35] Such a shift relative to the unsubstituted Pc is even higher, being about 0.7 V.[19]

Anions derived from $Cu^{II}(F_{64}Pc)$ exhibit a relatively enhanced solubility in organic solvents vs complexes with $x < 64$ due to the presence of bulky perfluoroisopropyl substituents. The $(F_{64}Pc)^{\bullet 3-}$ radical trianion can be generated electrochemically, chemically using reducing agents, and by photochemical reduction using hydrazine hydrate ($E_{redox} = -0.01$ V vs SCE[36]) in dimethylformamide (DMF)[33] or in ethanol even without any added reductant.[16] Taken together, the results suggest that $F_{64}Pc$ is the strongest electron acceptor fluorinated phthalocyanine macrocycle reported to date.

The X-ray structures of the reduced species reveal the variations in molecular parameters induced by the addition of more electrons.

X-RAY CRYSTAL STRUCTURES

Two different views of the crystal structure of **1**, $\{cryptand(K^+)\}[Cu^{II}(F_{64}Pc)^{\bullet 3-}]^-\cdot 2C_6H_4Cl_2$, are shown in Figure 2, while the structures of $\{cryptand(K^+)\}_2[Cu^{II}(F_{64}Pc^{4-})]^{2-}$, crystallized with solvent, **2**, and without it, **3**, are shown in Figure 3. The packing diagrams of two unit cells of **1**–**3**, viewed along the crystallographic axes, are shown in Figure S1, Supporting Information.

The X-ray structures unambiguously determine the compositions listed in Table 1. Monoanions of $Cu^{II}(F_{64}Pc)$ are present in **1**, whereas dianions are present in **2** and **3**. The overall shape of the Pcs is nonplanar, with some twisting of benzene rings by about 17° in **1** and a slight doming of the macrocycle. The departure of Pc from planarity, combined with the steric hindrance of the peripheral *iso*-alkyl substituents, impacts molecular packing (see also Figure S1).

The related $[Cu^{II}(F_xPc^{\bullet 3-})]^-$ and $[Cu^{II}(F_xPc)^{4-}]^{2-}$ anions ($x = 8, 16$), with the same charges as the anions with $x = 64$ but with only aromatic F substituents tend to form closely packed architectures and π-stacks, or chains with $\pi-\pi$ interactions, features that affect their optical and magnetic properties.[28,29] A different situation is observed for **1**–**3**, based on $[Cu^{II}(F_{64}Pc)^{n-}]^{(n-2)-}$ ($n = 3, 4$) anions.

The $[Cu^{II}(F_{64}Pc)^{\bullet 3-}]^-$ anions in **1** form chessboard-like layers in which macrocycles alternate with the cryptand(K^+) cations (Figure 2a). Short van der Waals F $(C_3F_7)\cdots F$ (C_3F_7)

https://doi.org/10.1021/acs.inorgchem.3c00887
Inorg. Chem. 2023, 62, 11390−11401

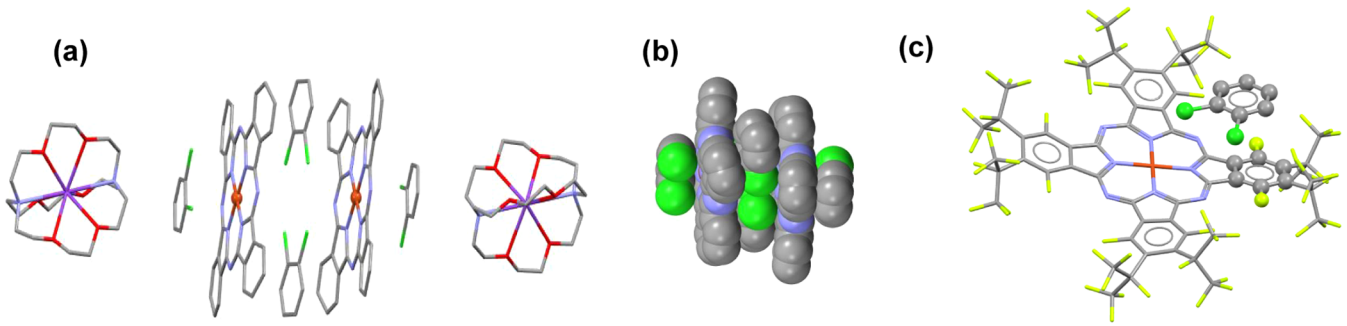

Figure 4. Simplified view of the aromatic solvent interactions with the Pc in **1**. (a) The assembly of the cations, Pc, and *o*-dichlorobenzene located within the "bivalve", shell-like cavity formed by the concave sides of Pcs, termed "interior" solvents, as well as on the convex sides, termed "exterior" solvents, are shown. The distances between the "exterior" solvents and the Pc coordination plane reach a low 3.25 Å, which is shorter than the 3.35 Å value for the graphite crystal interplanar distance, but this interaction did not result in its identification by the aromaticity test as π-stacking.[39] Hydrogens and Pc substituents have been omitted for the sake of clarity. (b) Space-filling representation of the assembly of panel (a) but with cations and Pc substituents omitted for the sake of clarity. (c) Ball-and-stick representations of one of the two aromatic interactions between an "interior" *o*-dichlorobenzene and a benzene ring of the Pc. The stacking, ∼3.9 Å, is termed as "strong", reaching about ∼90% of the maximum strength[39] (see also Figure S5 and Table S1 for the complete list of strong interactions).

Table 2. Bond Lengths Observed via X-ray Diffraction in Fluorinated Copper Phthalocyanines[a]

Compound[reference]	Charge state of the Pc	Average bond lengths, Å			
		Cu−N_{pyr}	C−N_{pyr}	C−N_{meso} Δshort/long	C−F average
$Cu^{II}(F_8Pc^{2-})$[40]	−2	1.939(5)	1.375(8)	1.313(8)/1.341(8) 0.028	1.352(7)
{cryptand(Na^+)}[$Cu^{II}(F_8Pc^{\bullet 3-})$]$^-$ [29]	−3	1.9536(17)	1.377(3)	1.312(3)/1.352(3) 0.040	1.360(2)
{Bu_4N^+}$_2$[$Cu^{II}(F_8Pc^{4-})$]$^{2-}$·2$C_6H_4Cl_2$[28]	−4	1.961(5)	1.386(8)	1.283(8)/1.374(8) 0.091	1.381(7)
$Cu^{II}(F_{16}Pc^{2-})$[41]	−2	1.952(2)	1.378(3)	1.320(3)/1.323(2) 0.003	1.346(2) 1.341(2)
[$Cu^{II}(F_{16}Pc^{\bullet 3-})$]$^-$ in $(PPN^+)_3[Cu(F_{16}Pc)]_3^{3-}$·2$C_6H_5CN$[29]	−3	1.954(2)	1.377(2)	1.325(2)/1.328(2) 0.003	1.345(2)
[$Cu^{I}(F_{16}Pc^{2-})$]$^-$ in $(PPN^+)_3[Cu(F_{16}Pc)]_3^{3-}$·2$C_6H_5CN$[29]	−2	1.955(2)	1.378(2)	1.326(2)/1.329(2) 0.003	1.345(2)
{cryptand(Na^+)}$_2$[$Cu^{II}(F_{16}Pc^{4-})$]$^{2-}$ [28]	−4	1.954(2)	1.383(2)	1.305(2)/1.363(2) 0.058	1.348(2)
$Cu^{II}(F_{64}Pc^{2-})$·2$C_4H_8O_2$ (**0**) [23]	−2	1.958(3)	1.365(5)	1.326(5)/1.324(5) 0.002	1.344(5)* 1.370(5)** 1.331(5)′
{cryptand(K^+)}[$Cu^{II}(F_{64}Pc^{\bullet 3-})$]$^-$·2$C_6H_4Cl_2$ (**1**) this work	−3	1.948(3)	1.375(5)	1.333(5)/1.319(5) 0.014	1.343(5)* 1.368(5)** 1.330(5)′
{cryptand(K^+)}$_2$[$Cu^{II}(F_{64}Pc^{4-})$]$^{2-}$·$C_6H_4Cl_2$ (**2**) this work	−4	1.954(3)	1.382(4)	1.363(5)/1.297(5) 0.066	1.344(5)* 1.367(5)** 1.331(6)′
{cryptand(K^+)}$_2$[$Cu^{II}(F_{64}Pc^{4-})$]$^{2-}$ (**3**) this work	−4	1.956(2)	1.382(2)	1.370(2)/1.293(2) 0.077	1.342(2)* 1.370(2)** 1.323(2)′

[a]*, **, and ′ show C−F bonds with different fluorine atoms in the $F_{64}Pc$ macrocycle (as shown in Figure 1).

contacts of 2.6−2.9 Å are present, indicating a contribution to packing. No π−π interactions between Pc cores are present in **1**.

The Pc layers are separated by bulky cryptand(K^+) cations and *o*-dichlorobenzene molecules (Figure 2b). Unlike **1**, the [$Cu^{II}(F_{64}Pc^{4-})$]$^{2-}$ dianions are isolated (noninteracting) in **2** and **3**. The large voids are occupied by cryptand(K^+) cations. Note that molecular aggregations are suppressed by *iso*-C_3F_7 groups irrespective of the metal center of M($F_{64}Pc$), viz. M = Cu^{II}, Co^{II}, Zn^{II}, and $V^{IV}O$.[13,17,23,38] Interestingly, the intermolecular interactions of {cryptand-(K^+)}$_2$[$Cu^{II}(F_{64}Pc^{4-})$]$^{2-}$ appear sufficiently plastic to allow its crystallization with and without solvent, **2** and **3**, respectively, but the solvent ability to participate in π−π interactions with Pcs may play a role in packing. Indeed, π-type interactions are detected in **1** (Figure 4c) between the solvents, nested in the concave sides of the Pcs, and the benzene rings of the Pcs (Figures 4a and 2b). Such interactions are not present in **2**.

The stable, 18 π-electron aromaticity is largely lost by the formation of less stable 19 and 20 π-electron systems. The addition of electrons, combined with fluorinated substituent

https://doi.org/10.1021/acs.inorgchem.3c00887
Inorg. Chem. 2023, 62, 11390−11401

accretion, has structural consequences. A comparison of geometric features of **0**, **1**, **2**, and **3** reveals these effects (Table 2).

Six coordination via axial solvent binding appears common for crystals of ($F_{64}Pc$) M = Cu^{II}, Co^{II}, Zn^{II}, $V^{IV}O$.[13,17,23,34] A reduced, four-coordination, square-planar geometry is observed for **1**−**3**, the copper(II) ions being located almost exactly in the center of the average plane formed by the four N_{pyr} atoms. The Cu displacement from this plane is only 0.014 Å for **1**, 0.022 Å for **2**, but 0.000 for **3**. The Cu−N bond distances do not vary significantly, despite the fact that the Cu is six-coordinated in **0** but four-coordinated in **1**−**3**. The most statistically significant changes are observed for the lengths of the N_{meso}−C bonds.[30,31,42−45] Shorter and longer N_{meso}−C bonds, relative to the parent macrocycle, $Cu^{II}(F_{64}Pc)$, for which the bonds are the same, are present in the reduced macrocycles with x = 8, 16. The common pattern is illustrated in Figure 5.

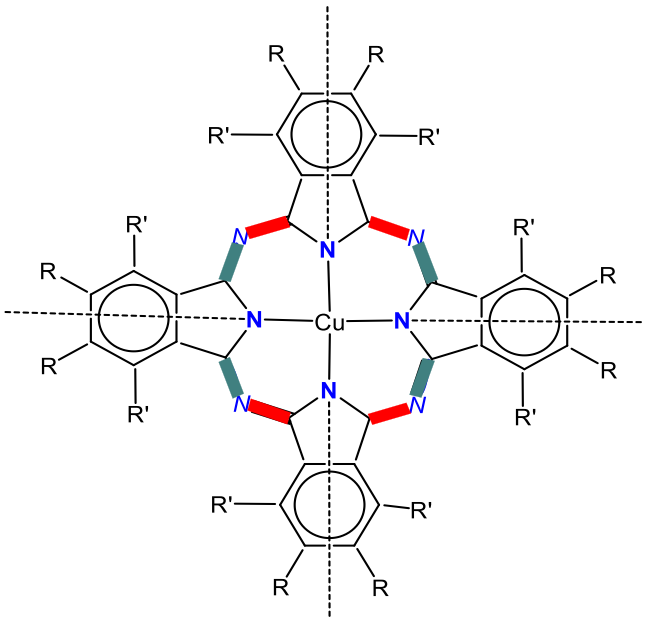

Figure 5. Schematic illustration of the distortions listed in Table 2. *N* and **N** are the meso and pyrrolic N atoms, respectively. R = F or C_3F_7. R′ = H or F. Bond elongation and shortening, relative to the parent $Cu^{II}(F_{64}Pc^{2-})\cdot 2C_4H_8O_2$, are shown as red and green bars, respectively. The dotted lines mark the location of mirror and C_2 symmetry elements. Although the pyrrolic C−N bonds are shown as single, their observed lengths are statistically indistinguishable, suggesting sp^2 delocalization.

The fourfold rotational axis of the nonreduced molecule is reduced to a twofold one. This axis and the two mirror planes (also C_2 axes) occur due to the equivalency of the trans pyrrolic C−N bonds (Figure 5). The Δ value (difference between shorter and longer N_{meso}−C bonds) increases with the Pc negative charge when the number of F is constant, as observed for the $[Cu^{II}(F_{16}Pc)^{n-}]^{(n-2)-}/[Cu^{II}(F_8Pc)^{n-}]^{(n-2)-}$ (n = 3, 4) pairs.[28,29] For x = 64, Δ increases from 0.014 Å for $[Cu^{II}(F_{64}Pc^{\bullet 3-})]^-$ to 0.066−0.077 Å for $[Cu^{II}(F_{64}Pc^{4-})]^{2-}$ (Table 2). Moreover, the Δ values for $[Cu^{II}(F_8Pc)^{n-}]^{(n-2)-}$ (n = 3, 4) are larger than those for $[Cu^{II}(F_{16}Pc)^{n-}]^{(n-2)-}$ and $[Cu^{II}(F_{64}Pc)^{n-}]^{(n-2)-}$ (n = 3, 4), consistent with the higher electronic deficiency of the $F_{16}Pc$ and $F_{64}Pc$[19,20,23] macrocycles in comparison with the F_8Pc macrocycle. In general, the Pc macrocycles are more distorted in **2** and **3** relative to **1**.

A notable elongation of the C−F bonds was observed in a reduced $Cu^{II}(F_8Pc)$ macrocycle, but those lengths were not affected by the reductions in $Cu^{II}(F_{16}Pc)$.[28,29] $Cu^{II}(F_{64}Pc)$ has different types of C−F bonds, but all of them remained nearly unchanged by reductions.

The coordination environment of copper(II) centers in monoanionic copper(II) phthalocyanines $\{Cu^{II}(F_xPc)^{\bullet 3-}\}^-$ (x = 8, 16, 64) was also analyzed by utilizing the SHAPE 2.1 software, which is based on the continuous shape measure (CShMs) algorithm of Pinsky and Avnir.[49] The values given by the program tend to zero if the coordination sphere of a metal center forms a particular perfect reference polyhedron. Conversely, large values indicate strong deviations from the ideal geometry. In this case, we compare the observed geometry with an ideal square-planar geometry of copper(II) centers. The calculated coefficients are very small: 0.016 for x = 8, 0.000 for x = 16, and 0.005 for x = 64, indicating a nearly ideal square-planar geometry with D_{4h} symmetry in all three cases.

OPTICAL PROPERTIES

The UV−vis−near-infrared (NIR) spectra of parent $Cu^{II}(F_{64}Pc)$ and anionic salts **1** and **2**, obtained using KBr pellets prepared under Ar, are shown in Figure 6.

The increase in the fluorine content results in bathochromic shifts, consistent with the data obtained in solution.[37] $Cu^{II}(F_{64}Pc^{2-})(C_4H_8O_2)_2$ (**0**) exhibits Soret and Q-band maxima at 363 and 696 nm, respectively. For anions, the reduction of $Cu^{II}(F_8Pc)$ and $Cu^{II}(F_{16}Pc)$ was accompanied by a hypsochromic shift of the Q-bands.[28] $Cu^{II}(F_{64}Pc)$ behaves differently. The ligand-only reduction is most clearly defined in the Zn complex. Thus, $(Cl^-)[Zn(F_{64}Pc^{2-})]^0$ exhibits strong bands at 430 and 692 nm in DMF. The photochemical reduction of this solution led to the gradual formation of the $[Zn^{II}(F_{64}Pc^{\bullet 3-})]^-$ anions, with Q-band maxima at 468, 594, and 743 nm.[37,46] The photochemical reduction of $Zn(F_{64}Pc)$ in ethanol,[16] and electrochemical reduction of both $Zn(F_{64}Pc)$ and $Cu(F_{64}Pc)$ in trifluorotoluene[19] had the same spectroscopic effect. In the case of **1**, the intensity of the 695 nm band decreases relative to $Cu^{II}(F_{64}Pc)$, and new bands appear at 426, 592, and 777 nm (Figure 6 and Table 3). The same set of bands is observed in the spectrum of $[Zn^{II}(F_{64}Pc^{\bullet 3-})]^-$, thus supporting the formation of $F_{64}Pc^{\bullet 3-}$. The spectroscopy of **2**, the doubly reduced $[Cu^{II}(F_{64}Pc^{4-})]^{2-}$ is more complex, spectral data for the tetraanion $(F_{64}Pc)^{4-}$ being reported here for the first time. The Q-bands split in **2** giving rise to new bands in the visible region. Some splitting in the Soret region, as well as a hypsochromic shift, is also noted, effects that are similar to those observed for other Pc^{4-} tetraanions.[50]

Weak NIR absorptions of the radical anion and dianion are present at 868−871 and 1005−1006 nm, consistent with bands observed for all reduced phthalocyanines,[30,31,42,43,51] including $[Zn^{II}(F_{64}Pc^{\bullet 3-})]^-$,[16] and tetrapyrazinoporphyrazine[42−45] macrocycles. Such bands are more intense relative to those of **1** and **2**, but the bands for the related $Cu^{II}(F_8Pc)$ and $Cu^{II}(F_{16}Pc)$ are also weak (see Table 3).[28,29]

In addition to the Soret and Q-bands, charge-transfer (CT) bands are also noted. Such bands, usually broad, are caused by the $\pi-\pi$ interaction between the macrocycles, in stacks or chains, as noted for the unhindered $[Cu^{II}(F_xPc)^{n-}]^{(n-2)-}$ (x = 8, 16; n = 3, 4) anions,[28,29] consistent with the tendency of

https://doi.org/10.1021/acs.inorgchem.3c00887
Inorg. Chem. 2023, 62, 11390−11401

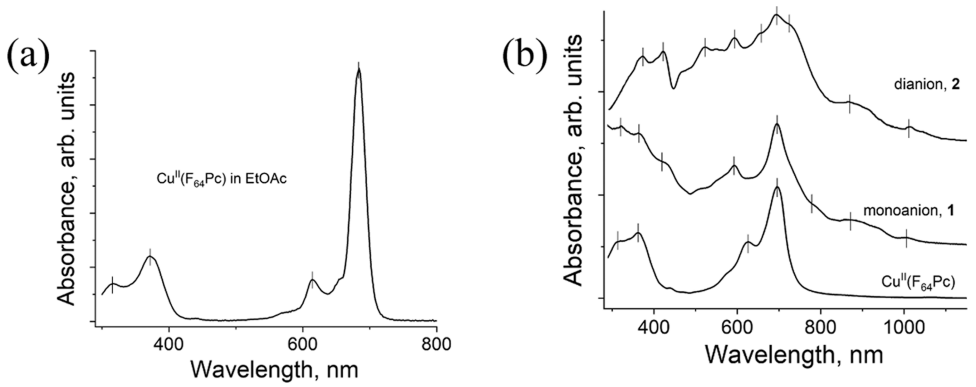

Figure 6. UV−vis−NIR spectra of $Cu^{II}(F_{64}Pc)$ and its reduced species. (a) Solution spectrum of **0** in ethyl acetate and (b) solid-state spectra of $Cu^{II}(F_{64}Pc)$, salts **1** and **2** in the KBr pellet. Vertical bars are used to mark spectral features. Absorbances are in arbitrary units. The absorption bands are listed in Table 3.

Table 3. UV−vis−NIR Data of Fluorinated Phthalocyanines and Reduced Complexes[a]

Compound	n in $Pc^{(2+n)-}$	Absorption band λ_{max} [nm], sh: shoulder, m; most intense peak in the Q-band		
		Soret band	Q-band	NIR
$Cu^{II}(F_8Pc)$[28]	0	332	612(m), 682, 735	1080 weak
$\{A\}[Cu^{II}(F_8Pc^{3\bullet-})]^-$ [28]	1	317	574	821, 923, 1625 (CT)
$\{Bu_4N^+\}_2[Cu^{II}(F_8Pc^{4-})]^{2-}\cdot 2solv$[29]	2	319	590	1013
$Cu^{II}(F_{16}Pc)$[28]	0	339	628(m), 789	1137 weak
$(PPN^+)_3[Cu(F_{16}Pc)]_3^{3-}\cdot 2C_6H_5CN$[29]	1	324	571	912, 1414 (CT)
$\{A\}_2[Cu^{II}(F_{16}Pc^{4-})]^{2-}$ [28]	2	324	544(m), 623(sh)	833, 934, 1670 (CT)
$Cu^{II}(F_{64}Pc^{2-})\cdot$2-ethyl acetate, **0**	0	319, 363	626, 696(m)	
$Cu^{II}(F_{64}Pc)$ (in ethyl acetate), **0**	0	318, 372	614, 684(m)	
$[Zn^{II}(F_{64}Pc^{\bullet 3-})\cdot$2-ethanol][16]	1	452	452, 589, 695 729 (m)	924,1038
$\{B\}[Cu^{II}(F_{64}Pc^{\bullet 3-})]^-\cdot$2solv, **1**	1	320, 363, 426 (sh)	592, 695(m), 777(sh)	871, 1006
$\{B\}_2[Cu^{II}(F_{64}Pc^{4-})]^{2-}\cdot$solv, **2**	2	373, 422	523, 594, 656(sh) 695(m), 720(sh)	868, 1005

[a]CT: charge-transfer band; A: cryptand(Na^+); B: cryptand(K^+); solv: $C_6H_4Cl_2$; and PPN^+: bis(triphenylphosphine)iminium.

Table 4. EPR and Magnetic Data (Superconducting Quantum Interference Device (SQUID)) for Reduced $Cu^{II}(F_xPc)$ Complexes and the Parent Nonreduced Complex, x = 64[a]

Complex Cu:Pc spins	Magnetics			EPR
	Magn. moment (μ_B)	Weiss temp. (K)	Magnetic exchange interaction constant J (cm^{-1})	$A_{\|}$, ΔH: mT
$\{A\}[Cu^{II}(F_8Pc^{\bullet 3-})]^-$ 1/2:1/2	2.39	− 9	intra-dimer J_{R-R} = −21.8 inter-dimer J_{R-R} = −14.6 J_{Cu-R} = −10.8, J_{Cu-Cu} = −1.5, T = max of magn. suscept. at 9 K	IS; HFI below 155 K; 298 K: g = 2.1652, ΔH = 95.02
$\{B\}[Cu^{II}(F_8Pc^{4-})]^{2-}\cdot$2solv 1/2:0	1.60	−4		298 K: $g_{\|}$ = 2.097, $A_{\|}$ = 26.56, $g_{\perp}$ = 1.9628
$\{C\}[Cu(F_{16}Pc)]_3^{3-}\cdot 2C_6H_5CN$ pairs of $[Cu^{II}(F_{16}Pc)^{\bullet 3-}]^-$ separated by diamagnetic $[Cu^{I}(F_{16}Pc)^{2-}]^-$ [28]	3.25	−21.5	J_{inter} = −16.3	an EPR signal was not observed
S = [(1/2 + 1/2) + (1/2 + 1/2)] separated by (0 + 0)			J_{intra} = −5.6	
$\{A\}_2[Cu^{II}(F_{16}Pc)^{4-}]^{2-}$[29] 1/2:0	1.95	−1		298 K: $g_{\|}$ = 2.1806, $A_{\|}$ = 20.11, $g_{\perp}$ = 1.9597 4.2 K: $g_{\|}$ = 2.1638, $A_{\|}$ = 21.66, $g_{\perp}$ = 1.9586
$Cu^{II}(F_{64}Pc^{2-})(C_4H_8O_2)_2$, powder, **0** 1/2:0	spin only	0	0	4.5 K: $g_{\|}$ = 2.1650, $A_{\|}$ = 23.00, $g_{\perp}$ = 2.036, $A_{\perp}$ = 2.85
$Cu^{II}(F_{64}Pc)$ in ethanol,[23] **0** 1/2:0				4.5 K: $g_{\|}$ = 2.1855, $A_{\|}$= 22.11, $g_{\perp}$ = 2.0484, $A_{\perp}$= 2.18
$\{D\}[Cu^{II}(F_{64}Pc^{\bullet 3-})]^-\cdot$2solv, **1** 1/2:1/2	2.55	−1	J_{intra} = −0.56	IS 298 K: g_1 = 2.1723, ΔH_1 = 33.2, g_2 = 1.9514, ΔH_2 = 80.4
$\{D\}_2[Cu^{II}(F_{64}Pc^{4-})]^{2-}\cdot$solv, **2** 1/2:0				4.2 K: g_1 = 2.1154, ΔH_1 = 13.3, g_2 = 2.0617, ΔH_2 = 72.7

[a]{A}: {cryptand(Na^+)}; {B}: $(Bu_4N^+)_2$; {C}: $(PPN^+)_3$; {D}: {cryptand(K^+)}; solv: $C_6H_4Cl_2$; J_{intra}/k_B: Cu(II):$Pc^{\bullet 3-}$ radical; J_{inter}/k_B= intermolecular coupling; HFI: hyperfine interaction of the unpaired electron on Cu^{II} atoms with the nuclear spin of ^{63}Cu and ^{65}Cu (I = 3/2); IS: intermediate signal of Cu^{II} and $(F_8Pc)^{\bullet 3-}$; R: radical.

https://doi.org/10.1021/acs.inorgchem.3c00887
Inorg. Chem. 2023, 62, 11390−11401

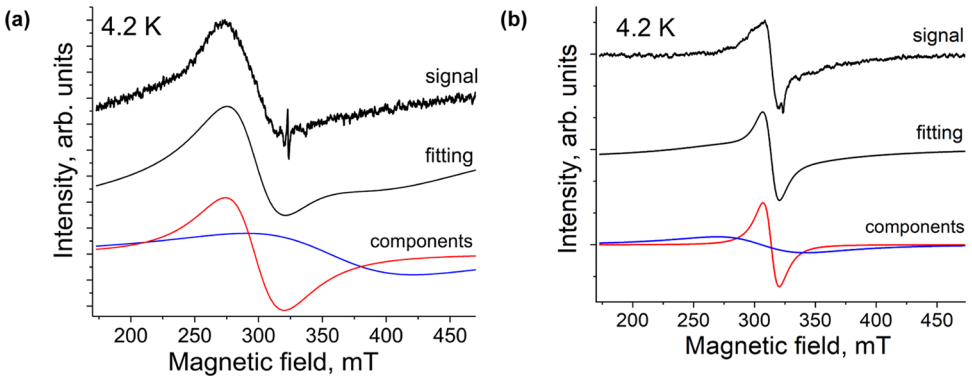

Figure 7. EPR spectra of polycrystalline (a) complex **1**; the g and ΔH components, g_1 = 2.1769, ΔH_1 = 46.1 mT, g_2 = 1.8176, ΔH_2 = 130.7 mT observed at 4.2 K were attributed to both Cu^{II} and $F_{64}Pc^{\bullet 3-}$; (b) complex **2**; the g and ΔH components, g_1 = 2.1154, ΔH_1 = 13.3 mT; g_2 = 2.0617, ΔH_2 = 72.7 mT at 4.2 K were attributed to Cu^{II}.

fluorinated macrocycles with aromatic fluorine substituents to aggregate via π-stacking. However, the introduction of eight, bulky perfluoroisopropyl substituents, in the peripheral positions of Pc, led to molecular isolation of $F_{64}Pc$ macrocycles in $M^{II}F_{64}Pc$.[13,17,23,38] Since the isolation in the solid state is enhanced upon reduction due to the presence of bulky cryptand(K^+) counterions, CT bands beyond 1100 nm are not observed for any reduced $F_{64}Pc$.

MAGNETIC INTERACTIONS AND F EFFECTS

Relationships between the electronic and structural properties of reduced $F_{64}Pc$ species, especially given the possible simultaneous presence of unpaired electrons on both metal and ligand centers, are revealed by paramagnetic resonance and magnetic properties, summarized in Table 4.

Insights into the electronic structure of the reduced species, exhibiting unpaired spins located in both metal and ligand frontier orbitals, are provided by magnetic resonance. Information on the ligand-located spins was provided by the solution EPR of $[Zn(F_{64}Pc^{\bullet 3-})]^-$.[16,37,46] The X-band CW−EPR spectrum of the ethanol solution of photo-reduced $Zn^{II}(F_{64}Pc)$, the Zn analogous of $Cu^{II}(F_{64}Pc)$, reveals a g = 2.003 broad signal, attributed to $[Zn^{II}(F_{64}Pc^{\bullet 3-})]^-$, the Zn analog of **1**. The same signal is obtained upon chemical reduction. No intermolecular magnetic couplings are detected, an observation relevant to the magnetic interactions possible when diamagnetic Zn(II) is replaced by paramagnetic Cu(II). Conversely, magnetic resonance studies of $Cu^{II}(F_{64}Pc)$ reveal the features of a spin located exclusively on the coordinated metal center, as opposed to exclusively on the Pc ring, like in the previous case.

X-band CW−EPR (Table 4) and ENDOR of solid, magnetically undiluted **0**, and its solutions in ethanol, established the noninteracting nature of the Cu spins. Hyperfine couplings have also been revealed. The results have been corroborated by density functional theory computations.[23] Taken together, these findings regarding single-spin complexes are to be compared with cases when two spins are present simultaneously, i.e., reduced species.

The reduction of fluorinated $Cu^{II}(F_xPc)$ (x = 8, 16) phthalocyanines is mainly ring-centered, and accompanied by the formation of $[Cu^{II}(F_xPc)^{\bullet 3-}]^-$ and $[Cu^{II}(F_xPc)^{4-}]^{2-}$ anions.[28,29]

The EPR spectra of **1** exhibit a broad, asymmetric signal, which can be fitted well by two broad Lorentzian lines (Figures 7a and S2). At 270 K, a signal with g_1 = 2.2144 (ΔH_1 = 30.3 mT) and g_2 = 1.9949 (ΔH_2 = 63.8 mT) is observed (Figure S2). This signal originates from paramagnetic Cu^{II} and $F_{64}Pc^{\bullet 3-}$ species. These signals are different from those originating from individual Cu^{II} and $F_{64}Pc^{\bullet 3-}$ species. Thus, according to the g-factor value, Cu^{II} has a larger contribution to the g_1 line, but the hyperfine splitting (HFS) characteristic of isolated Cu^{II} is not observed. The g_2 line has a large contribution from $F_{64}Pc^{\bullet 3-}$, but this line is too broad to be assigned to the isolated $F_{64}Pc^{\bullet 3-}$ species. These observations can be explained by the existence of a weak exchange interaction between the Cu^{II} and $F_{64}Pc^{\bullet 3-}$ species. The g-factor (Figure S3a) and the linewidth of the signal (Figure S3b) are strongly temperature-dependent, getting broader and smaller, respectively, as the temperature decreases. At 4.2 K, a signal with g_1 = 2.1769 (ΔH_1 = 46.1 mT) and g_2 = 1.8176 (ΔH_2 = 130.7 mT) is observed (Figure 7). These data also support a weak, antiferromagnetic coupling. Previously, a symmetric broad signal with g = 2.1652 (ΔH = 95.02 mT) at room temperature was observed for $[Cu^{II}(F_8Pc^{\bullet 3-})]^-$ mono-anions.[29]

The low-temperature EPR signal of **2**, for which the ligand is diamagnetic, can also be fitted well by two Lorentzian lines with g_1 = 2.1154 (ΔH_1 = 13.3 mT) and g_2 = 2.0617 (ΔH_2 = 72.7 mT) at 4.2 K (Figure 7b). The observed parameters are close to those of $[Cu^{II}(F_xPc)^{4-}]^{2-}$ (x = 8, 16) anions with spins localized exclusively on the Cu^{II} ions. However, in these cases, a HFS is noted, unlike the signals of **2**, which lack HFS. The line with larger g_1 could be attributed to the parallel component of the signal, while the line with smaller g_2 could be attributed to the perpendicular component.[23,28] However, in the absence of EPR measurement of oriented single crystals, these attributions remain tentative.

Further insights into the electronic interactions are afforded by variable temperature static magnetic susceptibility measurements (Table 4 and Figure 8).

A spin-only value of the magnetic moment, in the absence of the Pc radical in **0**, results in a Curie paramagnet, i.e., Weiss temperature Θ = 0 K, indicating the absence of intermolecular Cu(II)−Cu(II) magnetic coupling.[23] Magnetic moments close to the spin-only value of 1.73 μ_B are characteristic of the copper(II) complexes, but larger values up to 2.2 μ_B are attainable due to orbital contributions.[47,48] In contrast to **0**, the effective magnetic moment of **1**, 2.55 μ_B ($\chi_M T$ is 0.81 emu·K/mol) at 300 K (Figures 8 and S4a), is close to the value of 2.45

https://doi.org/10.1021/acs.inorgchem.3c00887
Inorg. Chem. 2023, 62, 11390−11401

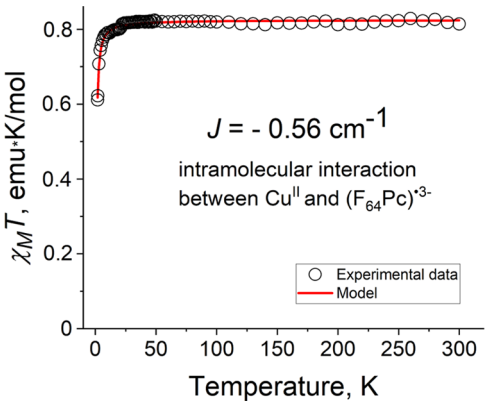

Figure 8. Temperature dependence of $\chi_M T$ for **1** and its modeling.

μ_B calculated for two noninteracting $S = 1/2$ spins and smaller than the 2.83 μ_B value expected for a triplet state.

The effective magnetic moment and $\chi_M T$ value of **1** remain constant down to ∼20 K, and then decrease (Figures 8 and S4a). The temperature dependence of the reciprocal molar magnetic susceptibility (Figures 8 and S4) is linear over the whole temperature range. The observed Weiss temperature, $\Theta = -1$ K, indicates a weak antiferromagnetic spin coupling.

The magnetic behavior of **1** was modeled using the PHI program[52] to estimate the degree of magnetic coupling. The shortest Cu−Cu distance, ∼7.5 Å, is too long from a magnetic point of view for a reasonable intermolecular, through-space coupling, leaving the intramolecular coupling between the $F_{64}Pc^{\bullet 3-}$ radical and the d^9 electron to be the dominant interaction. A good fitting of the experimental data (Figure 8) using $g(Cu^{II}) = 2.19$ and $g = 2.0000$ for $F_{64}Pc^{\bullet 3-}$ yielded $J = -0.56$ cm^{-1}. The ligand-only $g = 2.0000$ value is consistent with $g = 2.003-2.009$ measured for the solution, ligand-only signal of $[Zn(F_{64}Pc^{\bullet 3-})]^-$.[16,44] Compared with $F_{64}Pc^{\bullet 3-}$, the intramolecular couplings between Cu^{II} and $F_xPc^{\bullet 3-}$, $x = 8$ and 16, namely, −10.8 and −5.6 cm^{-1}, respectively (Table 4) are at least 1 order of magnitude larger.[28,29] As the degree of fluorination increases, the intramolecular magnetic coupling decreases, a trend consistent with the notion of enhanced spin density transfer to acceptor fluoro-substituents as x increases. Thus, the weakest coupling in $[Cu^{II}(F_{64}Pc)^{\bullet 3-}]^-$ could be explained by the extreme electron deficiency of its Pc core.[20,23] The geometry around the copper(II) atoms most probably does not affected the J values since, according to the SHAPE 2.1,[49] estimation, for all three anions with $x = 8$, 16, and 64, the geometry of copper(II) is very close to square-planar, D_{4h} symmetry. As a control experiment, the possibility of inter-Pcs coupling, mediated by the π-stacked solvents, was considered. Thus, the magnetic coupling was modeled with two J's, but values with reasonable accuracy could not be obtained. J is too small for such manipulations.

In summary, magnetic measurements confirm the existence of magnetically isolated molecules, but subject to intramolecular spin coupling that is the lowest among the copper $F_xPc^{\bullet 3-}$ species, as per an inverse correlation between its magnitude and x.

CONCLUSIONS

New, crystalline salts based on 1- and 2-electron reductions of copper(II) 1,4,8,11,15,18,22,25-octafluoro-2,3,9,10,16,17,23,24-octakisperfluoro(isopropyl) phthalocyanine ($Cu^{II}F_{64}Pc$) were obtained, and their crystal and molecular structures were elucidated. There are no intermolecular $\pi-\pi$ stacking interactions present, but such interactions are present between the Pc and the *o*-dichlorobenzene solvent of crystallization. The ligands are slightly twisted and form domes.

The Cu−N bonds are similar, and so are the benzene, pyrrolic, and all C−F bonds, with small variations. The major effect of reductions is the variation of $N_{meso}-C$ bonds, bonds that are equal in $Cu^{II}(F_xPc)$ except for $x = 8$. The reduced macrocycles exhibit alternative shortening and elongations of these bonds, resulting in the reduction of the fourfold axis to a twofold one.

This effect, linked to the partial loss of aromaticity when 19 and 20 π-electron complexes are formed, is more pronounced for the dianions $[Cu^{II}(F_{64}Pc^{4-})]^{2-}$ vs monoanions $[Cu^{II}(F_{64}Pc^{\bullet 3-})]^-$. Anionic species of $Cu^{II}(F_{64}Pc)$ and $Cu^{II}(F_{16}Pc)$, which contain highly electron-deficient Pc ligands, exhibit a smaller departure from bond equivalency and alternation in comparison with $Cu^{II}(F_8Pc)$, which has a relatively diminished electronic deficient Pc ligand.

Structural, optical, and magnetic studies reveal that the reduction along the series $[Cu^{II}(F_xPc)^{\bullet 3-}]^-$ and $[Cu^{II}(F_xPc)^{4-}]^{2-}$ (x = 8, 16, 64) mono- and dianions is mainly localized on the macrocycle. The only exception is $(PPN^+)_3[Cu(F_{16}Pc)]_3^{3-}\cdot 2C_6H_5CN$ complex, in which both the reduced macrocycle $[Cu^{II}(F_{16}Pc)^{\bullet 3-}]^-$ and the reduced metal center $[Cu^{I}(F_{16}Pc)^{2-}]^-$species co-exist.[29]

New, weak bands appear in the NIR, while bands in the visible region shift and split. The first reduction leads to $[Cu^{II}(F_xPc^{\bullet 3-})]^-$ species with two $S = 1/2$ spins localized on Cu^{II} atoms and delocalized over the F_xPc macrocycle. Coupling between these two spins decreases in order $[Cu^{II}(F_8Pc^{\bullet 3-})]^-$, $[Cu^{II}(F_{16}Pc^{\bullet 3-})]^-$, and $[Cu^{II}(F_{64}Pc^{\bullet 3-})]^-$ when the number of fluorine atoms increases. Most probably, the electron-withdrawing substituents have a crucial effect in stabilizing the anions. Monoanions $[Cu^{II}(F_xPc)^{\bullet 3-}]^-$ (x = 8, 16) with fluorine atoms attached directly to the Pc core form mainly closely packed π-stacks. The $[Cu^{II}(F_{64}Pc)^{\bullet 3-}]^-$ anions are isolated due to the presence of bulky perfluoroisopropyl substituents on the periphery that completely suppress any intermolecular interactions. The $[Cu^{II}(F_xPc)^{4-}]^{2-}$ (x = 8, 16, 64) dianions contain diamagnetic and EPR silent tetraanion macrocycles and paramagnetic Cu^{II} atoms with $S = 1/2$ spin state.

This work showed that $[Cu^{II}(F_{64}Pc^{2-})]$ could be a promising, solution-processable acceptor component in constructing air-stable donor−acceptor assemblies, including via strong $\pi-\pi$ stacking interactions with small donors. As such, the biradical nature of its monoanion complexes constitutes an attractive target for designing robust, magnetic, and probably conducting materials.

EXPERIMENTAL SECTION

Materials and Methods. Copper(II) 1,4,8,11,15,18,22,25-octafluoro-2,3,9,10,16,17,23,24-octakisperfluoro(isopropyl) phthalocyanine {$Cu^{II}(F_{64}Pc)$} was obtained as described.[23] 4,7,13,16,21,24-Hexaoxa-1,10-diazabicyclo[8.8.8]hexacosane (cryptand, Acros Organics) and potassium graphite (KC_8, Strem) were used as received. Solvents were purified under an argon atmosphere. *o*-Dichlorobenzene ($C_6H_4Cl_2$) was distilled over CaH_2 under reduced pressure; *n*-hexane was distilled over Na/benzophenone. The solvents were degassed and stored in a glovebox that contained less than 1 ppm of water and oxygen. The crystals of **1**−**3** were stored in the glovebox.

https://doi.org/10.1021/acs.inorgchem.3c00887
Inorg. Chem. 2023, 62, 11390−11401

Table 5. X-ray Diffraction Data for 1−3

compound	1	2	3
emp. formula	$C_{86}H_{44}Cl_4CuF_{64}KN_{10}O_6$	$C_{92}H_{72}CuF_{64}K_2N_{12}O_{12}$ (+ squeezed one $C_6H_4Cl_2$ molecule)	$C_{92}H_{72}CuF_{64}K_2N_{12}O_{12}$
M_r (g/mol)	2773.75	2895.35	2895.35
color and shape	black prism	black, prismatic	black plate
crystal system	triclinic	triclinic	triclinic
space group	$P\bar{1}$	$P\bar{1}$	$P\bar{1}$
a (Å)	17.0999(8)	16.3374(5)	13.3077(5)
b (Å)	18.2638(8)	19.0573(6)	15.1963(5)
c (Å)	19.3623(9)	20.9513(7)	15.2534(5)
α (deg)	113.1521(16)	78.7461(12)	70.5040(12)
β (deg)	111.3183(16)	79.0264(11)	83.4840(13)
γ (deg)	95.6638(17)	68.6512(11)	71.3761(13)
V (Å^3)	4969.2(4)	5907.6(3)	2755.45(17)
Z	2	2	1
ρ_{calc} (g/cm^3)	1.854	1.628	1.745
μ (mm^{-1})	0.549	0.417	0.447
$F(000)$	2740	2894	1447
T (K)	100(2)	100(2)	100(2)
max. 2Θ (deg)	50.118	51.456	57.314
reflns measured	69 600	80 229	40 239
unique reflns	17 620	22 486	14 169
parameters	1549	1871	852
restraints	0	73	15
reflns[$F_o > 2(F_o)$]	13 440	16 114	11 432
$R_1[F_o > 2\sigma(F_o)]$	0.0602	0.0643	0.0388
WR_2 (all data)	0.1246	0.1780	0.1018
G.O.F.	1.048	1.053	1.043
CCDC number	2238185	2238187	2238186

KBr pellets for IR- and UV−vis−NIR measurements were also prepared in the glovebox. EPR (**1** and **2**) and SQUID measurements (**1**) were performed on polycrystalline samples sealed in 2 mm quartz tubes under an ambient pressure of argon gas.

Syntheses and Crystallization of 1−3. The salt {cryptand(K$^+$)}[Cu^{II}(F$_{64}$Pc$^{\bullet 3-}$)]$^-$·2C$_6$H$_4$Cl$_2$ (**1**) was obtained via the reduction of Cu^{II}(F$_{64}$Pc) (25 mg, 0.012 mmol) in the presence of one equivalent of cryptand (4.8 mg, 0.012 mmol) and an excess of potassium graphite (20 mg, 0.148 mmol) at 60 °C in 16 mL of *o*-dichlorobenzene and stirred for 24 h, under inert atmosphere.

The deep-blue solution formed was cooled to 25 °C, and potassium graphite was removed by filtering the solution into a 50 mL glass tube of 1.8 cm diameter with a ground glass plug, followed by the careful layering of 30 mL of *n*-hexane. Large, black prismatic crystals, formed after 1−2 months in a 20% yield, were washed with *n*-hexane. No other types of crystals formed, as revealed by the microscopic examination of crystals and unit cell determinations for several specimens. Calculated for $C_{86}H_{44}Cl_4N_{10}O_6F_{64}KCu$: C, 37.21; H, 1.59; N, 5.05. Found: C, 36.89; H, 2.01; N, 5.19.

The salt {cryptand(K$^+$)}$_2$[Cu^{II}(F$_{64}$Pc^{4-})]$^{2-}$·C$_6$H$_4$Cl$_2$ (**2**) was obtained via the reduction of Cu^{II}(F$_{64}$Pc) (25 mg, 0.012 mmol) in the presence of one equivalent of cryptand (4.8 mg, 0.012 mmol) and using an excess of potassium graphite (20 mg, 0.148 mmol) at 60 °C in 16 mL of *o*-dichlorobenzene, under inert atmosphere. After the deep-blue solution was stirred for 24 h, one more equivalent of cryptand (4.8 mg, 0.012 mmol) and an excess of potassium graphite (20 mg, 0.148 mmol) were added. The solution turned red-purple while stirred for an additional 24 h. The mixture was cooled to room temperature, and the potassium graphite was filtered out. The clear solution was placed in a glass tube and carefully layered with *n*-hexane. After 1 month, several large crystals having the shape of elongated plates and weighing about 2 mg formed on the walls of the tube. A small amount of powder also formed at the bottom of the tube. The crystals were removed from the solvent via decanting, washed with several portions of *n*-hexane, and the solvent was decanted every time to remove any powder to yield pure crystals. Four large crystals were examined via X-ray diffraction, and the unit cell of **2** was confirmed in each case. These crystals were used for nondestructive EPR studies and for the determination of optical properties of **2**.

The crystals of {cryptand(K$^+$)}[Cu^{II}(F$_{64}$Pc)$^{\bullet 3-}$]$^-$ (**3**) were obtained via the reduction of Cu^{II}(F$_{64}$Pc) (25 mg, 0.012 mmol) in the presence of two equivalents of cryptand (9.6 mg, 0.024 mmol) and an excess of potassium graphite (20 mg, 0.148 mmol) at 60 °C in 16 mL of *o*-dichlorobenzene upon stirring for 24 h under inert atmosphere. The mixture was cooled to room temperature, and the potassium graphite was filtered out. The clear solution was placed in a glass tube and carefully layered with *n*-hexane. Crystals formed after 1 month. The crystals were isolated by decanting the solvents and subsequently washed with several portions of *n*-hexane. Most crystals were large prisms with the cell parameters of **1**. Several small black plates, easily distinguishable from the large prisms under microscopic examination, were separated manually (Pasteur method). All plates were tested by X-ray diffraction and shown to belong to only one crystal phase with the cell parameters of **3**.

General Methods. UV−vis−NIR, EPR and SQUID Magnetic Measurements. UV−vis−NIR spectra were measured in KBr pellets on a PerkinElmer Lambda 1050 spectrometer in the 250−2500 nm range. EPR spectra were recorded for the polycrystalline samples of **1** and **2** with a JEOL JES-TE 200 X-band ESR spectrometer equipped with a JEOL ES-CT470 cryostat. A Quantum Design MPMS-XL SQUID magnetometer was used to measure the static magnetic susceptibility of **1** at a 1 kOe magnetic field in cooling and heating conditions in the 300−1.9 K range. The sample-holder contribution and core temperature-independent diamagnetic susceptibility (χ_d) were subtracted from the experimental values. The χ_d values were estimated from the extrapolation of the data in the high-temperature range by fitting the data with the following expression: $\chi_M = C/(T - \Theta) + \chi_d$, where C is the Curie constant and Θ is the Weiss temperature. Effective magnetic moments (μ_{eff}) were calculated with the formula $\mu_{eff} = (8\chi_M T)^{1/2}$.

https://doi.org/10.1021/acs.inorgchem.3c00887
Inorg. Chem. 2023, 62, 11390−11401

X-ray Crystal Structure Determination and Analyses. X-ray diffraction data for **1**−**3** are listed in Table 5. The X-ray diffraction data for complexes **1**−**3** were obtained on a D8 Venture diffractometer (Bruker, Germany) in the ϕ- and ω-scanning modes at the center of the shared equipment, Kurnakov Institute of General and Inorganic Chemistry, Russian Academy of Sciences (λ = 0.71073 Å, Incoatec IμS 3.0 microfocus X-ray source). Primary indexing, the refinement of unit cell parameters, and the integration of reflections were performed using the Bruker APEX3 software package.[53] The reflection intensities were corrected for absorption using the SADABS software.[54] The structures were solved by direct methods[55] and refined by the full-matrix least-squares techniques against F^2 using the program suite.[56,57]

Nonhydrogen atoms were refined in the anisotropic approximation, except for some fluorine and carbon atoms in disordered parts of trifluoromethyl groups. Equivalent fluorine−carbon distances in these molecular fragments were restrained to be approximately equal by applying SADI restraints, as well as thermal displacement parameters were restrained by using the SIMU instruction at the refinement. All hydrogen atoms were placed in calculated positions, riding on the nonhydrogen atoms to which they were bonded. Three perfluoroisopropyl groups are disordered between two orientations with 0.650(3)/0.350(3), 0.650(3)/0.350(3), and 0.803(5)/0.197(5) occupancies in **2**. In the crystal structure of **2**, there is one highly disordered *o*-dichlorobenzene molecule, one molecule of solvent is present per unit cell, which was squeezed using the standard Olex2/PLATON routine.[58] One $-CH_2-CH_2-O-CH_2-CH_2-O-CH_2-CH_2-$ group of cryptand(K^+) cation and the fluorine atoms of one CF_3 group are disordered over two orientations with 0.925(5)/0.075(5) and 0.930(4)/0.070(4) occupancies in **3**. Structural visualizations, aromaticity calculations, and intermolecular interactions have been obtained using the Mercury package.[39]

■ ASSOCIATED CONTENT

Supporting Information

The Supporting Information is available free of charge at https://pubs.acs.org/doi/10.1021/acs.inorgchem.3c00887.

Packing diagrams, EPR, magnetics, and π interactions for new compounds (PDF)

Accession Codes

CCDC 2238185, 2238187, and 2238186 (compounds **1**, **2**, and**3**, respectively) contain the supporting crystallographic data for this paper. These data can be obtained free of charge via www.ccdc.cam.ac.uk/data_request/cif, or by emailing data_request@ccdc.cam.ac.uk, or by contacting The Cambridge Crystallographic Data Centre, 12 Union Road, Cambridge CB2 1EZ, U.K.; fax: +44 1223 336033.

■ AUTHOR INFORMATION

Corresponding Authors

Maxim A. Faraonov − *Federal Research Center of Problems of Chemical Physics and Medical Chemistry, Russian Academy of Sciences, Chernogolovka 142432, Russia;* orcid.org/0000-0003-0805-601X; Email: maksimfaraonov@yandex.ru

Sergiu M. Gorun − *Department of Chemistry and Biochemistry and Center for Functional Materials, Seton Hall University, South Orange, New Jersey 07079, United States;* orcid.org/0000-0003-1719-4086; Email: sergiu.gorun@shu.edu

Dmitri V. Konarev − *Federal Research Center of Problems of Chemical Physics and Medical Chemistry, Russian Academy of Sciences, Chernogolovka 142432, Russia;* orcid.org/0000-0002-7326-8118; Email: konarev3@yandex.ru

Authors

Ilya A. Yakushev − *Kurnakov Institute of General and Inorganic Chemistry, Russian Academy of Sciences, Moscow 119991, Russia*

Evgeniya I. Yudanova − *Federal Research Center of Problems of Chemical Physics and Medical Chemistry, Russian Academy of Sciences, Chernogolovka 142432, Russia*

Marius Pelmus − *Department of Chemistry and Biochemistry and Center for Functional Materials, Seton Hall University, South Orange, New Jersey 07079, United States;* orcid.org/0000-0001-5913-8168

Akihiro Otsuka − *Division of Chemistry, Graduate School of Science, Kyoto University, Kyoto 606-8502, Japan;* orcid.org/0000-0002-3141-0702

Hideki Yamochi − *Division of Chemistry, Graduate School of Science, Kyoto University, Kyoto 606-8502, Japan*

Hiroshi Kitagawa − *Division of Chemistry, Graduate School of Science, Kyoto University, Kyoto 606-8502, Japan;* orcid.org/0000-0001-6955-3015

Complete contact information is available at: https://pubs.acs.org/10.1021/acs.inorgchem.3c00887

Notes

The authors declare no competing financial interest.

■ ACKNOWLEDGMENTS

This work was supported by the Russian Science Foundation (project no. 21-73-10207). The UV−vis−NIR spectra were obtained with the support of the Ministry of Science and Higher Education of the Russian Federation (registration number AAAA-A19-119092390079-8). The magnetic measurements at low temperatures were acquired with funding from JSPS KAKENHI (Grant Numbers JP20K05448, JP20H05623, and JP22H02157). The work in the United States was supported by the Center for Functional Materials, Seton Hall University.

■ REFERENCES

(1) McKeown, N. B. Phthalocyanine Materials: Synthesis, Structure, and Function. *Chemistry of Solid State Materials*; Cambridge University Press: Cambridge, U.K., 1998.

(2) Leznoff, C. C.; Lever, A. B. P. *Phthalocyanines: Properties and Applications*; VCH: Weinheim, 1989; pp 1−4.

(3) Wöhrle, D.; Schnurpfeil, G.; Makarov, S. G.; Kazarin, A.; Suvorova, O. N. Practical Applications of Phthalocyanines - from Dyes and Pigments to Materials for Optical, Electronic and Photo-Electronic Devices. *Macroheterocycles* **2012**, *5*, 191−202.

(4) Zeis, R.; Siegrist, T.; Kloc, C. Single-Crystal Field-Effect Transistors Based on Copper Phthalocyanine. *Appl. Phys. Lett.* **2005**, *86*, No. 022103.

(5) Bao, Z.; Lovinger, A. J.; Brown, J. New Air-Stable *n*-Channel Organic Thin Film Transistors. *J. Am. Chem. Soc.* **1998**, *120*, 207−208.

(6) de Boer, R. W. I.; Stassen, A. F.; Craciun, M. F.; Mulder, C. L.; Molinari, A.; Rogge, S.; Morpurgo, A. F. Ambipolar Cu- and Fe-Phthalocyanine Single-Crystal Field-Effect Transistors. *Appl. Phys. Lett.* **2005**, *86*, No. 262109.

(7) Klyamer, D.; Bonegardt, D.; Basova, T. Fluoro-Substituted Metal Phthalocyanines for Active Layers of Chemical Sensors. *Chemosensors* **2021**, *9*, 133−162.

(8) Ray, A. K.; Mukherjee, D.; Sarkar, S. Phthalocyanines: A Class of Organic Photoconductive Materials. In *Photoconductivity and Photoconductive Materials: Fundamentals, Techniques and Applications, Volume 1: Fundamentals*; Kasap, S. O., Ed.; John Wiley & Sons, 2022; Vol. *21*, pp 831−852.

(9) Sorokin, A. B. Catalytic Transformations in the Presence of Metal Phthalocyanine Complexes and Their Analogs. *Handbook of Porphyrin Science*; World Scientific Publishing Company, 2016; Vol. *36*−*40*, pp 193−322.
(10) Santos, K. L. M.; Barros, R. M.; da Silva Lima, D. P.; Nunes, A. M. A.; Sato, M. R.; Faccio, R.; de Lima Damasceno, B. P. G.; Oshiro, J. A., Jr. Prospective Application of Phthalocyanines in the Photodynamic Therapy against Microorganisms and Tumor Cells: A Mini-Review. *Photodiagn. Photodyn. Ther.* **2020**, *32*, No. 102032.
(11) Lever, A. B. P.; Milaeva, E. R.; Speier, G. *Phthalocyanines: Properties and Applications*; VCH Publishers: New York, 1993; Vol. 3.
(12) Minnes, R.; Weitman, H.; Lee, H.-J.; Gorun, S. M.; Ehrenberg, B. Enhanced Acidity, Photophysical Properties and Liposome Binding of Perfluoroalkylated Phthalocyanines Lacking C-H Bonds. *Photochem. Photobiol.* **2006**, *82*, 593.
(13) Bench, B. A.; Beveridge, A.; Sharman, W. M.; Diebold, G. J.; van Lier, J. E.; Gorun, S. M. Introduction of Bulky Perfluoroalkyl Groups at the Periphery of Zinc Perfluorophthalocyanine: Chemical, Structural, Electronic, and Preliminary Photophysical and Biological Effects. *Angew. Chem., Int. Ed.* **2002**, *41*, 747.
(14) Loas, A.; Gerdes, R.; Zhang, Y.; Gorun, S. M. Broadening the Reactivity Spectrum of a Phthalocyanine Catalyst While Suppressing Its Nucleophilic, Electrophilic and Radical Degradation Pathways. *Dalton Trans.* **2011**, *40*, 5162.
(15) Gerdes, R.; Lapok, L.; Tsaryova, O.; Wöhrle, D.; Gorun, S. M. Rational Design of a Reactive yet Stable Organic-Based Photocatalyst. *Dalton Trans.* **2009**, 1098.
(16) Moons, H.; Loas, A.; Gorun, S. M.; Van Doorslaer, S. Photoreduction and Light-Induced Triplet-State Formation in a Single-Site Fluoroalkylated Zinc Phthalocyanine. *Dalton Trans.* **2014**, *43*, 14942−14948.
(17) Bench, B. A.; Brennessel, W. W.; Lee, H.-J.; Gorun, S. M. Synthesis and Structure of a Biconcave Cobalt Perfluorophthalocyanine and Its Catalysis of Novel Oxidative Carbon-Phosphorus Bonds Formation by Using Air. *Angew. Chem.* **2002**, *114*, 776−780.
(18) Drozd, D.; Szczubiałka, K.; Łapok, Ł.; Skiba, M.; Patel, H.; Gorun, S. M.; Nowakowska, M. Visible Light Induced Photosensitized Degradation of Acid Orange 7 in the Suspension of Bentonite Intercalated with Perfluoroalkyl Perfluoro Phthalocyanine Zinc Complex. *Appl. Catal., B* **2012**, *125*, 35−40.
(19) Nagel, S.; Lener, M.; Keil, C.; Gerdes, R.; Łapok, Ł.; Gorun, S. M.; Schlettwein, D. Electrochromic Switching of Evaporated Thin Films of Bulky, Electronic Deficient Metallo-Phthalocyanines. *J. Phys. Chem. C* **2011**, *115*, 8759−8767.
(20) Nguyen, T. H. Q.; Pelmuş, M.; Colomier, C.; Gorun, S. M.; Schlettwein, D. The Influence of Intermolecular Coupling on Electron and Ion Transport in Differently Substituted Phthalocyanine Thin Films as Electrochromic Materials: A Chemistry Application of the Goldilocks Principle. *Phys. Chem. Chem. Phys.* **2020**, *22*, 7699−7709.
(21) Keil, C.; Tsaryova, O.; Lapok, L.; Himcinschi, C.; Wöhrle, D.; Hild, O. R.; Zahn, D. R. T.; Gorun, S. M.; Schlettwein, D. Growth and Characterization of Thin Films Prepared from Perfluoro-Isopropyl-Substituted Perfluorophthalocyanines. *Thin Solid Films* **2009**, *517*, 4379−4384.
(22) Weissbecker, J.; Loas, A.; Gorun, S. M.; Schlettwein, D. Switching of the Rate-Limiting Step in the Electrochromic Reduction of Fluorinated Phthalocyanine Thin Films by Decreased Intermolecular Coupling. *Electrochim. Acta* **2015**, *157*, 232−244.
(23) Moons, H.; Łapok, Ł.; Loas, A.; Van Doorslaer, S.; Gorun, S. M. Synthesis, X-Ray Structure, Magnetic Resonance, and DFT Analysis of a Soluble Copper(II) Phthalocyanine Lacking C−H Bonds. *Inorg. Chem.* **2010**, *49*, 8779−8789.
(24) Konarev, D. V.; Kuzmin, A. V.; Khasanov, S. S.; Batov, M. S.; Otsuka, A.; Yamochi, H.; Kitagawa, H.; Lyubovskaya, R. N. Salts with Titanyl and Vanadyl Phthalocyanine Radical Anions. Molecular Design and Effect of Cations on the Structure and Magnetic and Optical Properties. *CrystEngComm* **2018**, *20*, 385.
(25) Inabe, T.; Tajima, H. Phthalocyanines − Versatile Components of Molecular Conductors. *Chem. Rev.* **2004**, *104*, 5503.
(26) Yu, D. E. C.; Matsuda, M.; Tajima, H.; Kikuchi, A.; Taketsugu, T.; Hanasaki, N.; Naito, T.; Inabe, T. Variable Magnetotransport Properties in the TPP$[Fe(Pc)L_2]_2$ System (TPP = Tetraphenylphosphonium, Pc = Phthalocyaninato, L = CN, Cl, and Br). *J. Mater. Chem.* **2009**, *19*, 718.
(27) Matsuda, M.; Yoshida, G.; Yamaura, J.; Inabe, T.; Tajima, H. The Magnetoresistance Effect in a Conducting Molecular Crystal Consisting of Dicyano(phthalocyaninato)manganese(III). *Dalton Trans.* **2017**, *46*, 1892.
(28) Konarev, D. V.; Faraonov, M. A.; Batov, M. S.; Andronov, M. G.; Kuzmin, A. V.; Khasanov, S. S.; Otsuka, A.; Yamochi, H.; Kitagawa, H.; Lyubovskaya, R. N. Effect of Reduction on the Molecular Structure and Optical and Magnetic Properties of Fluorinated Copper(II) Phthalocyanines. *Dalton Trans.* **2020**, *49*, 16821−16829.
(29) Konarev, D. V.; Troyanov, S. I.; Kuzmin, A. V.; Nakano, Y.; Ishikawa, M.; Faraonov, M. A.; Khasanov, S. S.; Litvinov, A. L.; Otsuka, A.; Yamochi, H.; Saito, G.; Lyubovskaya, R. N. The Salts of Copper Octafluoro- and Hexadecafluorophthalocyanines Containing $[Cu^{II}(F_8Pc)^{4-}]^{2-}$ Dianions and $[CuF_{16}Pc]^-$ Monoanions. *Inorg. Chem.* **2017**, *56*, 1804−1813.
(30) Konarev, D. V.; Faraonov, M. A.; Kuzmin, A. V.; Khasanov, S. S.; Nakano, Y.; Norko, S. I.; Batov, M. S.; Otsuka, A.; Yamochi, H.; Saito, G.; Lyubovskaya, R. N. Crystalline Salts of Metal Phthalocyanine Radical Anions $[M(Pc^{3-})]^-$ (M = Cu^{II}, Pb^{II}, $V^{IV}O$, $Sn^{IV}Cl_2$) with Cryptand(Na^+) Cations: Structure, Optical and Magnetic Properties. *New J. Chem.* **2017**, *41*, 6866−6874.
(31) Konarev, D. V.; Kuzmin, A. V.; Faraonov, M. A.; Ishikawa, M.; Khasanov, S. S.; Nakano, Y.; Otsuka, A.; Yamochi, H.; Saito, G.; Lyubovskaya, R. N. Synthesis, Structures, and Properties of Crystalline Salts with Radical Anions of Metal-Containing and Metal-Free Phthalocyanines. *Chem.—Eur. J.* **2015**, *21*, 1014−1028.
(32) Loutfy, R. O.; Hsiao, C. K.; Ong, B. S.; Keoshkerian, B. Electrochemical Evaluation of Electron Acceptor Materials. *Can. J. Chem.* **1984**, *62*, 1877−1885.
(33) Nafady, A.; Alsalme, A. M.; Al-Farhan, K. A.; El Khatib, R. M.; Bhargava, S. Probing Solvation and Ion-Pairing Effects on the Redox Behavior of Cyclopentadienyl Cobalt Dicarbonyl, CpCo(CO)2, in the Presence of $[B(C_6F_5)_4]^-$ Anion. *Int. J. Electrochem. Sci.* **2014**, *9*, 8131−8144.
(34) Carrión, E. N.; Loas, A.; Patel, H. H.; Pelmus, M.; Ramji, K.; Gorun, S. M. Fluoroalkyl Phthalocyanines: Bioinspired Catalytic Materials. *J. Porphyrins Phthalocyanines* **2018**, *22*, 371−397. and references therein
(35) Holmes, S. A.; Thomas, T. D. Electron Distribution in Trifluoromethylbenzenes. Electron Donation by the Trifluoromethyl Group. *J. Am. Chem. Soc.* **1975**, *97*, 2337−2341.
(36) Connelly, N. G.; Geiger, W. E. Chemical Redox Agents for Organometallic Chemistry. *Chem. Rev.* **1996**, *96*, 877−910.
(37) Keizer, S. P.; Mack, J.; Bench, B. A.; Gorun, S. M.; Stillman, M. J. Spectroscopy and Electronic Structure of Electron Deficient Zinc Phthalocyanines. *J. Am. Chem. Soc.* **2003**, *125*, 7067−7085.
(38) Łapok, Ł.; Lener, M.; Tsaryova, O.; Nagel, S.; Keil, C.; Gerdes, R.; Schlettwein, D.; Gorun, S. M. Structures and Redox Characteristics of Electron-Deficient Vanadyl Phthalocyanines. *Inorg. Chem.* **2011**, *50*, 4086−4091.
(39) Macrae, C. F.; Sovago, I.; Cottrell, S. J.; Galek, P. T. A.; McCabe, P.; Pidcock, E.; Platings, M.; Shields, G. P.; Stevens, J. S.; Towler, M.; Wood, P. A. Mercury 4.0: From Visualization to Analysis, Design and Prediction. *J. Appl. Crystallogr.* **2020**, *53*, 226−235.
(40) Matumoto, A.; Hoshino, N.; Akutagawa, T.; Matsuda, M. N-Type Semiconducting Behavior of Copper Octafluorophthalocyanine in an Organic Field-Effect Transistor. *Appl. Sci.* **2017**, *7*, No. 1111.
(41) Yoon, S. M.; Song, H. J.; Hwang, I.-C.; Kim, K. S.; Choi, H. C. Single Crystal Structure of Copper Hexadecafluorophthalocyanine ($F_{16}CuPc$) Ribbon. *Chem. Commun.* **2010**, *46*, 231−233.
(42) Faraonov, M. A.; Konarev, D. V.; Fatalov, A. M.; Khasanov, S. S.; Troyanov, S. I.; Lyubovskaya, R. N. Radical Anion and Dianion

https://doi.org/10.1021/acs.inorgchem.3c00887
Inorg. Chem. 2023, 62, 11390−11401

Salts of Titanyl Macrocycles with Acceptor Substituents or an Extended π-System. *Dalton Trans.* **2017**, *46*, 3547−3555.
(43) Faraonov, M. A.; Romanenko, N. R.; Kuzmin, A. V.; Konarev, D. V.; Khasanov, S. S.; Lyubovskaya, R. N. Crystalline Salts of the Ring-Reduced Tin(IV) Dichloride Hexadecachlorophthalocyanine and Octachloro- and Octacyanotetrapyrazinoporphyrazine Macrocycles with Strong Electron-Withdrawing Ability. *Dyes Pigm.* **2020**, *180*, No. 108429.
(44) Faraonov, M. A.; Osipov, N. G.; Romanenko, N. R.; Kuzmin, A. V.; Kornev, A. B.; Stuzhin, P. A.; Khasanov, S. S.; Konarev, D. V. Crystalline Salts of Anionic Free-Base Tetrapyrazinoporphyrazines with Alkyl-Substituents or an Extended π-Electron System. *New J. Chem.* **2022**, *46*, 22195−22202.
(45) Konarev, D. V.; Faraonov, M. A.; Kuzmin, A. V.; Osipov, N. G.; Khasanov, S. S.; Otsuka, A.; Yamochi, H.; Kitagawa, H.; Lyubovskaya, R. N. Molecular Structures, and Optical and Magnetic Properties of Free-Base Tetrapyrazinoporphyrazine in Various Reduction States. *New J. Chem.* **2019**, *43*, 19214−19222.
(46) Keizer, S. P.; Han, W.; Stillman, M. J. Photochemically-Induced Radical Reactions of Zinc Phthalocyanine. *Inorg. Chem.* **2002**, *41*, 353−358.
(47) Figgis, B. N.; Harris, C. M. 175. Magnetochemistry. Part III. Compounds of Bivalent Copper. *J. Chem. Soc.* **1959**, 855.
(48) Kato, M.; Jonassen, H. B.; Fanning, J. C. Copper(II) Complexes with Subnormal Magnetic Moments. *Chem. Rev.* **1964**, *64*, 99−128.
(49) (a) Llunell, M.; Casanova, D.; Cirera, J.; Alemany, P.; Alvarez, S. *Program SHAPE*, version 2.1; University of Barcelona: Spain, March, 2013. (b) Pinsky, M.; Avnir, D. Continuous Symmetry Measures. 5. The Classical Polyhedra. *Inorg. Chem.* **1998**, *37*, 5575−5582.
(50) Konarev, D. V.; Kuzmin, A. V.; Khasanov, S. S.; Litvinov, A. L.; Otsuka, A.; Yamochi, H.; Kitagawa, H.; Lyubovskaya, R. N. Dianionic Titanyl and Vanadyl $(Cation^{+})_2[M^{IV}O(Pc^{4-})]^{2-}$ Phthalocyanine Salts Containing Pc^{4-} Macrocycles. *Chem.—Asian J.* **2018**, *13*, 1552−1560.
(51) Konarev, D. V.; Kuzmin, A. V.; Khasanov, S. S.; Batov, M. S.; Otsuka, A.; Yamochi, H.; Kitagawa, H.; Lyubovskaya, R. N. Salts with Titanyl and Vanadyl Phthalocyanine Radical Anions. Molecular Design and Effect of Cations on the Structure and Magnetic and Optical Properties. *CrystEngComm* **2018**, *20*, 385−401.
(52) Chilton, N. F.; Anderson, R. P.; Turner, L. D.; Soncini, A.; Murray, K. S. PHI: A Powerful New Program for the Analysis of Anisotropic Monomeric and Exchange-Coupled Polynuclear *d* - and *f* -Block Complexes. *J. Comput. Chem.* **2013**, *34*, 1164−1175.
(53) Bruker. *APEX3, SAINT and SADABS*; Bruker AXS Inc.: Madison, 2016.
(54) Krause, L.; Herbst-Irmer, R.; Sheldrick, G. M.; Stalke, D. Comparison of Silver and Molybdenum Microfocus X-Ray Sources for Single-Crystal Structure Determination. *J. Appl. Crystallogr.* **2015**, *48*, 3−10.
(55) Sheldrick, G. M. *SHELXT* − Integrated Space-Group and Crystal-Structure Determination. *Acta Crystallogr., Sect. A: Found. Adv.* **2015**, *71*, 3−8.
(56) Sheldrick, G. M. Crystal Structure Refinement with *SHELXL*. *Acta Crystallogr., Sect. C: Struct. Chem.* **2015**, *71*, 3−8.
(57) Dolomanov, O. V.; Bourhis, L. J.; Gildea, R. J.; Howard, J. A. K.; Puschmann, H. *OLEX2*: A Complete Structure Solution, Refinement and Analysis Program. *J. Appl. Crystallogr.* **2009**, *42*, 339−341.
(58) Spek, A. L. *PLATON* SQUEEZE: A Tool for the Calculation of the Disordered Solvent Contribution to the Calculated Structure Factors. *Acta Crystallogr., Sect. C: Struct. Chem.* **2015**, *71*, 9−18.

https://doi.org/10.1021/acs.inorgchem.3c00887
Inorg. Chem. 2023, 62, 11390−11401